Polyoxometalate-Loaded Carboxymethyl Chitosan Nanoparticles with Anticancer Activity

Jaclyn M. Parris[‡,a], Giann Wiprächtiger[‡,a], Reyhaneh Hooshmandabbasi[b], Caroline Maake[*,b], Greta R. Patzke[*,a]

[a] Department of Chemistry, University of Zurich, Winterthurerstrasse 190, CH-8057 Zurich, Switzerland

[b] Institute of Anatomy, University of Zurich, Winterthurerstrasse 190, CH-8057 Zurich, Switzerland

KEYWORDS: Polyoxometalate, Nanoparticles, Anticancer Activity

ABSTRACT: Nanoparticles composed of selected polyoxometalates (POMs) and carboxymethyl chitosan (CMC) were prepared, characterized, and tested for anticancer activity to establish structure-activity relationships. Cell viability was investigated immediately after treatment and after 24 h to assess both cell recovery and delayed cytotoxicity. The study focused on three questions: (a) trends in cytotoxicity based on POM nuclearity and heteroatoms, (b) effects of CMC encapsulation strategies on cytotoxicity, and (c) cell viability after a recovery period. Among polyoxotungstates, $[NaP_5W_{30}O_{110}]^{14-}$, with a high tungsten content, showed the greatest cytotoxicity towards PC-3 cells at low concentrations. $[Co_4(H_2O)_2(PW_9O_{34})_2]^{10-}$ demonstrated moderate cytotoxicity with an IC_{50} of 437 ± 23 µM for MRC-5 cells, compared to 11 ± 0.3 µM for $[NaP_5W_{30}O_{110}]^{14-}$. Both POMs were encapsulated in a CMC matrix, forming nanoparticles of 100-250 nm, and analyzed by FT-IR and Raman spectroscopy, DLS, and cryo-TEM, and tested against MRC-5, PC-3, and HeLa cells. It was found that forming nanoparticles increased the magnitude of the cytotoxicity compared to the free POM, especially for the lower end of concentrations tested. Furthermore, we newly monitored the cell viability after a 24 h rest period without treatment, allowing for observations of delayed negative or positive effects on the cells. This thorough approach revealed that the preparative strategy applied for encapsulation of $[Co_4(H_2O)_2(PW_9O_{34})_2]^{10-}$ in CMC selectively influences the toxicity against HeLa and PC-3 cells compared to the normal MRC-5 cell line.

INTRODUCTION

Cancer is among the leading causes of early death in most countries.[1] Because of the persistence, the number of types, and the intrinsic heterogeneity of cancer, there is an unwavering need for effective anticancer agents.[2]

Currently, cis-diamminedichloroplatinum(II) (cisplatin) is one of the most widely used metal-based chemotherapeutics, as it is active against many types of cancers.[3,4,5,6] The efficiency of cisplatin continuously drives interest in selective, effective, and low-cost organometallic or metallodrugs.[7]

To this end, polyoxometalates (POMs) are attractive candidates for anticancer agents. POMs are polynuclear, anionic, metal-oxo clusters, typically composed of W, Mo, V, or Nb centers in their high oxidation states bridged by oxygen atoms.[8] Their exceptional compositional and structural variety makes their properties highly tunable,[9,10] and of interest for bio-applications.[11–16] $[NH_3Pr^i]_6[Mo_7O_{24}]$, for example, has been well explored for its anticancer activity It has been proposed that the activity of $[NH_3Pr^i]_6[Mo_7O_{24}]$ arises from the reduction and re-oxidation of molybdenum centers in the cells.[17–25] Although typically predicted to be less active than polyoxomolybdates,[8,25] polyoxotungstates have also been extensively investigated as anticancer agents.[13,14,26]

On the other hand, the application of POMs as bioactive agents can be hindered by their instability at physiological pH.[26–28] This makes evidencing and controlling the active species in the cells difficult.[29] Therefore, in this work, we screened diverse small (polyoxo)tungstates for their structure-dependent anticancer activity, namely Na_2WO_4, $[PW_{12}O_{40}]^{3-}$ $\{PW_{12}\}$, $[PW_9O_{34}]^{9-}$ $\{PW_9\}$, $[NaP_5W_{30}O_{110}]^{14-}$ ($\{NaP_5W_{30}\}$), and $[Co_4(H_2O)_2(PW_9O_{34})_2]^{10-}$ ($\{Co_4(PW_9)_2\}$).

The anticancer activity or cytotoxicity of the tungstate species, Na_2WO_4,[30–32] $Na_3[PW_{12}O_{40}]$,[25] $H_3[PW_{12}O_{40}]$,[33] $[AsW_9O_{34}]^{9-}$,[34,35] $[SbW_9O_{34}]^{9-}$,[36] $[\{Na(H_2O)_2\}_3\{Co(H_2O)\}_3(\alpha\text{-}B\text{-}SbW_9O_{33})_2]^{9-}$,[36] $[NaP_5W_{30}O_{110}]^{14-}$,[37–39] $[Co_4(H_2O)_2(PW_9O_{34})_2\}]^{10-}$,[40] and $[Cu_4(H_2O)_2(PW_9O_{34})_2\}]^{10-}$, have all been investigated before.[41] Further information can be found in the SI (Table **S2**). In this work, we go beyond these studies by investigating the protracted effects of the POMs by monitoring the cells after the treatment and in follow-up assays at least 24 h after the exposure. During this time interval, they are incubated in POM-free medium to allow for cell recovery. The test can also potentially assist in making hypotheses about the speciation/stability of POMs.

Along these lines, we conducted a more detailed comparison of the anticancer activity of the Preyssler-type POM, $\{NaP_5W_{30}\}$[37–39,42–44] and the sandwich-type POM, $\{Co_4(PW_9)_2\}$,[40] based on the following selection criteria: (a) both POMs exhibit stability at physiological pH,[26,45,46] (b) $\{NaP_5W_{30}\}$ serves as a model compound for high tungstate loading, (c) sandwich-type POMs, such as $\{Co_4(PW_9)_2\}$, offer the opportunity to investigate the influence of different transition metal ions, starting with cobalt centers in the following, as cobalt complexes have been of interest as anticancer agents.[47]

Previous works have introduced modifications to the core inorganic structure of the POM,[48,49] i.e. covalent functionalization and encapsulation, leading to improved bioactivity,[50,51] either by increasing the POM's bioavailability,[37,52] or stability,[53] or by directly increasing the POM's efficacy through enhancing toxicity towards cancer cells or reducing toxicity towards normal cells.[54–57] Such

modifications include the addition of biomolecules and other organic groups to the POM as well as the encapsulation of the POM in drug carriers,[11] such as liposomes,[58–60] and starch.[61–63]

In our case, we look at the effect of encapsulation into carboxymethyl chitosan (CMC) to improve the anticancer activity of the POM. Inorganic-organic hybrid materials have been of interest for a long time, such as core-shell structures formed by encapsulation in a polymer matrix.[64,65] One such hybrid material, POM and chitosan-based nanocomposites,[65] has previously attracted interest.[12,38] Chitosan is a low-cost, naturally derived linear polysaccharide of interest to the pharmaceutical industry,[66] as it is biocompatible and biodegradable.[67] It is synthesized by deacetylation of chitin, the second most frequently occurring natural polysaccharide.[66,68] Shah *et al*. explored the cytotoxicity of $(NH_4)_{14}[NaP_5W_{30}O_{110}]$ and chitosan nanocomposites with the $[NaP_5W_{30}O_{110}]^{14-}$ ion. Chitosan encapsulation increased the cytotoxicity towards HeLa cells.[38]

Chitosan's application is limited through being water-soluble only after the protonation of the amine groups below pH 6.[69,70] Carboxymethylation of the C-6 hydroxyl group or the amine of the chitosan affords the O-, N-, or N,O-CMC derivatives, which offer enhanced solubility under physiological conditions due to deprotonated carboxyl groups.[70] The negatively-charged CMC can be combined with POM and crosslinked with Ca^{2+} to obtain biologically active nanoparticles.

Regarding CMC, Geisberger *et al.* observed that nanocomposites combining CMC and $[Co_4(H_2O)_2(PW_9O_{34})_2]^{10-}$ (38-378 µM POM) led to minimal inhibitory effect against HeLa cells with incubation times ranging from 1 h to 48 h of incubation. For 48 h of incubation, the nanoparticles were less toxic than the pristine POMs for higher concentrations of POM (76-378 µM).[40,52] A complete list of CMC-{POM} studies can be found in the supplementary information (Table **S1**).

In this work, we utilized different crosslinked CMC nanosystems prepared according to two methods described in previous studies (Geisberger *et al.*[40,52] and Croce *et al.*[71]). This was done in search of underlying preparation-activity relations to account for the various activity profiles of CMC-POM nanoparticles, i.e. enhanced or reduced cytotoxicity. The methods apply different chitosan starting material with different molecular weights, degrees of deacetylation, and carboxymethylation, as well as a different stoichiometry of starting material. $\{NaP_5W_{30}\}$ and $\{Co_4(PW_9)_2\}$ POMs were encapsulated in CMC as described above and were structurally and spectroscopically characterized. Cytotoxicity tests were then performed against both normal (MRC-5) and cancerous (PC-3 and HeLa) cells to explore the selectivity of the nanoparticles as anticancer agents. We specifically investigated delayed effects of the treatment, thereby adding a key parameter for assessing and comparing the anticancer activity of POMs and their respective nanocomposites.

In summary, this work addresses the following three questions: (a) Does the polyoxotungstate size and the presence of transition metal atoms exert a decisive influence on the POM's cytotoxicity? (b) What influence do the encapsulation with CMC and the method applied for encapsulation have on the cytotoxicity of the resulting nanoparticles? (c) Can essential information be obtained from subsequent viability assays after a rest period in fresh medium?

EXPERIMENTAL SECTION

Materials: Sodium acetate (NaOAc, ≥99%), potassium acetate (KOAc, ≥99 %), potassium chloride (KCl, ≥99%), potassium nitrate (KNO_3, ≥99%) sodium phosphate dibasic (Na_2HPO_4, ≥99%), cobalt(II) acetate tetrahydrate ($Co(OAc)_2 \cdot 4H_2O$, reagent grade), sodium tungstate dihydrate ($Na_2WO_4 \cdot 2H_2O$, ≥99%)), phosphotungstic acid hydrate ($H_3O_{40}PW_{12} \cdot xH_2O$), phosphoric acid ($H_3PO_4$, 85 wt.% in H_2O), and hydrogen peroxide solution (H_2O_2, 30 wt.% in H_2O) were purchased from Sigma Aldrich (Buchs, Switzerland). Acetic Acid (CH_3COOH, 100%) was purchased from Merck (Darmstadt, Germany). Monochloroacetic acid ($ClCH_2COOH$, 99%, flakes) and Chitosan ($(C_6H_{11}NO_4)_n$), molecular weight: 100 – 300 kDa, >85% deacetylated were purchased from Acros Organics by Thermo Fisher Scientific (Geel, Belgium). Chitosan 90/5 ($(C_6H_{11}NO_4)_n$) was purchased from Heppe Medical Chitosan (Halle (Saale), Germany. (Sodium hydroxide (NaOH, pellets) and calcium chloride ($CaCl_2$, pure, granulated) were purchased from Honeywell (Seelze, Germany).

Ham's F-12K (Kaighn's) Medium, Dulbecco's Modified Eagle's Medium (D6429), Phosphate Buffered Saline, and 0.25% Trypsin-EDTA, were purchased from Gibco from Thermo Fisher. PrestoBlue™ Cell Viability Reagent was purchased from Invitrogen by Thermo Fisher Scientific. Fetal calf serum (FCS Gold ADD) was purchased from Bio&Sell, Feucht, Germany, and inactivated for 30 min at 56 °C. All cell lines were obtained from ATCC, Molsheim, France.

Instrumental: Nuclear magnetic resonance spectra (^{1}H- and ^{31}P-NMR) were recorded at 25 °C on a 400 MHz Bruker Avance Spectrometer (Billerica, USA) with CP-MAS technology. UV-vis absorption spectra were recorded with a Lambda 365+ Perkin-Elmer UV/Visible spectrometer and a Quartz SUPRASIL precision cell (10 mm). Attenuated total reflectance Fourier transform infrared (FT-IR) spectra were recorded on a Bruker VERTEX 70 spectrometer. Raman spectra were recorded on an inVia Raman microscope from Renishaw with a 785 nm laser. Powder X-Ray diffraction (XRD) patterns were recorded on a STOE STADI P diffractometer in transmission mode (flat sample holders, Ge-monochromator, and Cu or Mo $K_{\alpha1}$ radiation) with a position-sensitive detector. Thermogravimetric analysis (TGA) was performed on a Netzsch STA 449 F3 Jupiter instrument under an inert atmosphere of N_2. Hydrodynamic sizes and zeta-potentials were measured with a Zetasizer Nano ZS90 (ZEN3690, Malvern Instruments Ltd, Malvern, UK) using polystyrene disposable cuvettes (Sarstedt AG & Co, Germany) and Malvern disposable folded capillary cells, respectively. Transmission electron cryo-microscopy (cryo-TEM) was performed with a Thermo Fisher Glacios G2 microscope, equipped with a Flacon 4i direct detection camera for image acquisition. The suspension was washed and filtered before being transferred to a grid, blotted for four seconds with filter paper, and lastly frozen with liquid N_2. The fluorescence intensity measurements were recorded using Cytation 5 (Biotek Monochromator, Excitation: 560/10, Emission: 590/10).

Synthesis and characterization of starting materials:

$K_{12.5}Na_{1.5}[NaP_5W_{30}O_{110}] \cdot 21H_2O$ ({NaP_5W_{30}}) was synthesized according to literature.[72] 16.5 g $Na_2WO_4 \cdot 2H_2O$ (50.0 mmol) was dissolved in 15 mL of deionized H_2O, then acidified with 13 mL of 85% H_3PO_4 (190.0 mmol). The mixture was added to several autoclaves with 15 mL Teflon liners from Parr Instrument Company and heated overnight at 160 °C. After the solution was cooled to room temperature, the samples were combined, and 8 mL of deionized H_2O was added. The product was precipitated with 5.0 g KCl (67.1 mmol) then filtered and washed with 2 M KOAc and methanol. After drying, the product was recrystallized from 20 mL of hot H_2O. After 24 h, white crystals were collected and analyzed by FT-IR (Figure **S3**) and Raman spectroscopy (Figure **S11**), ^{31}P-NMR spectroscopy (Figure **S26**), powder XRD (Figure **S18**), and TGA (Figure **S20**).[42,72] Stability was investigated by ^{31}P-NMR spectroscopy (Figure **S29**).

$K_{10}[Co_4(H_2O)_2(PW_9O_{34})_2] \cdot 22H_2O$ ({$Co_4(PW_9)_2$}) was synthesized according to literature.[73] 11.0 g $Na_2WO_4 \cdot 2H_2O$ (33.3 mmol) and 60.0 mg Na_2HPO_4 (4.2 mmol) were dissolved in 35 mL H_2O and the pH was adjusted to 7 with acetic acid. The solution was then heated to boiling and refluxed. To the reaction mixture, a 10 mL aqueous solution of 209.0 mg $Co(OAc)_2 \cdot 4\ H_2O$ (8.4 mmol) was added dropwise. After 2 h under reflux, an excess of KOAc was added to the warm solution, and upon cooling a crystalline precipitate formed. The product was filtered off and washed with a concentrated solution of KNO_3, followed by 50% ethanol. The material was transferred to a vial and stirred twice in 5 mL of 40 ºC H_2O to wash off the pink by-product. Subsequently, the material was dissolved in 80 ºC H_2O and precipitated by adding excess KNO_3 followed by recrystallization from 80 ºC H_2O by cooling slowly to 5 ºC. Alternatively, $Na_{10}[Co_4(H_2O)_2(PW_9O_{34})_2]$ could be obtained by precipitation with excess NaCl and recrystallization.[45] The purple crystals were collected, air-dried, and characterized by FT-IR (Figure **S4**) and Raman spectroscopy (Figure **S12**), powder XRD (Figure **S19**), and TGA (Figure **S21**).[45,73,74] Stability was monitored by UV-vis absorbance spectroscopy (Figure **S30**).

Carboxymethyl chitosan (CMC-1 and CMC-2) was synthesized according to the procedure of Geisberger *et al.*[40,75] 5.0 g of chitosan (from Heppe Medical or Acros Organics) was suspended in a mixture of 50 mL of deionized H_2O and isopropanol (1:4) and alkalized with 6.8 g NaOH (16.9 mmol). The mixture was heated to 55 ºC in an oil bath and stirred for 1 h. Afterwards, 7.5 g monochloroacetic acid (7.9 mmol) dissolved in 10 mL of isopropanol was added over 0.5 h using a dropping funnel. The solution was stirred for an additional 3.5 h and quenched with 100 mL of ethanol (70%). The product was collected by filtration and washed several times with ethanol (70-90%) to remove residual salts and H_2O. The brown product was dried by lyophilization. CMC-**2** was prepared from chitosan from Acros Organics and then treated with H_2O_2 to degrade the polymer to a shorter molecular weight.[40,76] 1 g of this CMC was dissolved in 20 mL H_2O and treated with 0.8 mL of 30% H_2O_2 at 40 °C for 0.5 h. The product was precipitated by 80 mL of ethanol, filtered then washed with 70–94% ethanol. CMC-**1** and **2** were subsequently characterized by FT-IR spectroscopy (Figures **S5** and **S6**) and ^{1}H-NMR spectroscopy (Figures **S22** and **23**).[75,77,78]

Nanoparticle preparation and characterization:

CMC-{POM}-1 was prepared according to literature.[40,71] A stock solution of 8 mg/mL CMC-**1** was prepared either in milli-Q H_2O (pH 7.1 to 7.3, adjusted with 1 M HCl) or phosphate-buffered saline (PBS). Then the solution was filtered with a 0.45 µm syringe filter (Filtropour S). 1.0 mL of the CMC-**1** stock solution was combined with a 1.0 mL solution of {NaP_5W_{30}} or {$Co_4(PW_9)_2$} in Milli-Q H_2O, PBS, or cell culture medium. The POM solutions were prepared by serial dilution from a stock solution. The solution was stirred for 0.5 h before adding 0.4 mL of an aqueous solution of 31.5 mM $CaCl_2$ (1.4 mg, 12.6 µmol) dropwise with a syringe. The suspension was vigorously stirred for an additional 1 h. During this time, the suspension developed an opalescence. The nanoparticle suspensions were characterized by DLS (Table **S3** and **S18-S20**) and cryo-TEM (Figure **2**). Air-dried nanoparticles were characterized by FT-IR (Figures **S8** and **S9**) and Raman spectroscopy (Figures **S13** and **S14**) after separating the particles with 10,000 molecular weight cut-off centrifuge filters from Merck to confirm encapsulation of the POM.

CMC-{POM}-2 was prepared by dissolving 2.0 mg CMC-**2** (degraded) in 1.0 mL PBS or cell culture medium. {$Co_4(PW_9)_2$} solutions in cell culture medium or PBS were prepared by serial dilution from a stock solution of POM. 1 mL of the CMC stock solution was combined with 1.0 mL of the POM solution and stirred for 0.5 h. Then 0.25 mL of 18.0 mM $CaCl_2$ (0.5 mg, 4.5 µmol) in H_2O was added dropwise and stirred vigorously for 1 h, giving an opalescent suspension. The nanoparticle suspensions were characterized by DLS (Table **S3**, **S18, and S19**). Air-dried particles were characterized by FT-IR (Figure **S10**) and Raman spectroscopy (Figure **S15**) after separation of the nanoparticles with 10,000 molecular weight cut-off centrifuge filters from Merck to ensure encapsulation of the POM.

Cell culture: MRC-5 cells (normal human lung fibroblasts) and HeLa cells (human cervical adenocarcinoma) were cultured in Dulbecco's Modified Eagle's Medium with L-Glutamine and 10% heat-inactivated FCS and PC-3 cells (human prostate adenocarcinoma) in F-12K Nutrient mix with L-Glutamine with 10% heat-inactivated FCS. Cell lines were cultured in a T75 tissue culture flasks in a humidified atmosphere at 37 °C with 5% CO_2. The cells were split when the cells reached a confluency of around 90% by washing with PBS followed by trypsinization for up to 6 min with 0.25% Trypsin-EDTA.

PrestoBlue viability assay: The MRC-5 cells, HeLa cells, and PC-3 cells were seeded with a density of 6,500 cells per well in 96-well plates (Greiner) and incubated for 24 h under cell culture conditions. Following, the medium was replaced with 100 µL of POM or nanocomposites with concentrations ranging from 2,500 to 2 µM or comparable concentrations of reference species, Na_2WO_4, $Co(OAc)_2$, $CoCl_2$, $CaCl_2$, or CMC nanoparticles without POM in medium, and incubated for 24 h under cell culture conditions. After incubation, cells were washed two times with fresh medium and exposed to 10% PrestoBlue in medium for 1 h. The fluorescence intensity was recorded with the Cytation 5 plate reader using excitation and emission wavelengths of 530 and 590 nm, respectively. PrestoBlue was washed off three times with fresh medium and cells were cultured for an additional 24, 48, or 72 h under cell culture conditions. Then the PrestoBlue reading was performed

again. The cell viability was calculated as a percentage of untreated control cells. At least five replicates were performed, and the averages and standard deviations were taken after the removal of the highest and lowest values. Dose-response curves of the averages and standard deviations were then plotted with 95% confidence bands in OriginPro 2021. If necessary irregular values were hidden from the fitting.

Statistical analysis: One-way analysis of variance (ANOVA) and Duncan's multiple range test (DMRT) were performed for each concentration to determine the significance of the effect of the test species. P-values lower than 0.05 were considered significant and for DMRT an α value of 0.05 was used.

RESULTS AND DISCUSSION

SYNTHESIS AND CHARACTERIZATION

$\{NaP_5W_{30}\}$[72] and $\{Co_4(PW_9)_2\}$[73] were synthesized according to the literature. $\{NaP_5W_{30}\}$ has a wheel-shaped structure composed of 30-tungsten atoms, while $\{Co_4(PW_9)_2\}$ is a dimer of two $\{PW_9O_{34}\}$ units coordinated to four cobalt(II) atoms (Figure **1**). As previously stated, the first is of interest for its high tungsten load, while the second introduces additional transition metals to the investigation.

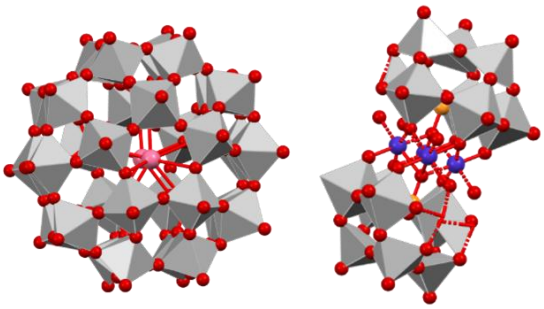

Figure 1. Polyhedral representation of $\{NaP_5W_{30}\}$ (left) and $\{Co_4(PW_9)_2\}$ (right) (grey = $\{WO_6\}$, red = O, yellow = P, pink = Na, and purple = Co).

As POMs can be unstable or present as different species in aqueous solution and under physiological conditions,[27–29,43,79] well-known stable POM species were taken as the focus of our investigation. However, stability and speciation tests in aqueous solution and cell culture media were still performed to verify the stability of $\{NaP_5W_{30}\}$ and $\{Co_4(PW_9)_2\}$.[26,45,46] $\{NaP_5W_{30}\}$ was dissolved in F-12K culture medium and monitored by ^{31}P-NMR spectroscopy over 96 h (Figure **S29**). The characteristic signal of $\{NaP_5W_{30}\}$ at -10.2 ppm was observed on day zero and day four, indicating the POM's stability. To investigate the stability of the paramagnetic $\{Co_4(PW_9)_2\}$, $\{Zn_4(PW_9)_2\}$ was used as an analogue.[40] $\{Zn_4(PW_9)_2\}$ was dissolved in DMEM cell culture medium and investigated after zero days and four days (Figure **S28**). The characteristic signal of $\{Zn_4(PW_9)_2\}$ at -4.8 ppm remained unchanged, while a second peak arising from phosphate in the medium shifted by -0.2 ppm by the fourth day. The presence of only one POM peak in each of the spectra suggests that $\{Zn_4(PW_9)_2\}$ and $\{NaP_5W_{30}\}$ are the only phosphate-containing POM species present in the corresponding medium. Alongside both POM stability experiments, the respective medium was also monitored by ^{31}P-NMR. No shifts were observed of the phosphate peak in the F-12K (Figure **S29**), while the peak in DMEM shifted by +0.2 ppm after 96 h, which may indicate that $\{Zn_4(PW_9)_2\}$ has some influence on the phosphate species in the medium (Figure **S28**).

The stability of $\{Co_4(PW_9)_2\}$ was also confirmed directly by UV-vis spectroscopy (Figure **S30**). $\{Co_4(PW_9)_2\}$ was dissolved in DMEM without phenol red and absorbance maxima were observed for the cobalt(II) transitions at 579 nm,[45] along with two shoulders at 514 and 499 nm. After 72 h, the position of the maxima remained unchanged. To check for the characteristic absorption peak of tungstate anions at 254 nm,[80] the solutions were diluted with PBS due to the overlapping absorbance of the DMEM. No shifts of the peak position were observed after 72 h. These results further indicate that $\{Co_4(PW_9)_2\}$ is stable in the cell culture medium.

Nanoparticles were prepared using two methods with different chitosan starting materials, one reported by Croce *et al.*,[71] and the other by Geisberger *et al.*[40] Encapsulated $\{Co_4(PW_9)_2\}$ and $\{NaP_5W_{30}\}$, formed stable nanoparticles typically with a hydrodynamic radius ranging from 100 to 250 nm and a zeta potential of approximately -20 mV (Tables **S3, S18**, and **S19**), depending on the POM concentration and the medium in which the nanocomposites are prepared.

The encapsulation of POMs in the CMC matrix was confirmed with FT-IR (Figures **S8**-**S10**) and Raman spectroscopy (Figures **S13**-**S15**). For the spectroscopic characterization of the nanoparticles, free POM was separated from the nanoparticle suspension using 10,000 molecular weight cut-off centrifuge filters and then air-dried. For each nanoparticle system, the characteristic vibrations of CMC and the respective POM are observed. The asymmetric and symmetric stretching vibrations of the COO^- group of CMC appear at 1579 and 1401 cm^{-1} in CMC-$\{NaP_5W_{30}\}$-**1** (Figure **S8**) and at 1589 and 1409 cm^{-1} in CMC-$\{Co_4(PW_9)_2\}$-**1** (the first peak also overlaps with N-H bending) (Figure **S9**).[69,81,82] The second peak is slightly shifted towards higher wave numbers than in the spectrum of the CMC polymer; this peak is also observed for the reference nanoparticles without POM, suggesting that the methoxy group of CMC is interacting with Ca^{2+} ions to form the nanoparticles. The peaks at 1320 cm^{-1} in CMC-$\{NaP_5W_{30}\}$-**1** and 1317 cm^{-1} in CMC-$\{Co_4(PW_9)_2\}$-**1** also arise from CMC and can be assigned to C-O stretching,[83] and the peaks at 1160 and 1064 cm^{-1} can be assigned to CH-OH stretching vibrations.[69,81] The peak at 1160 cm^{-1} in CMC-$\{NaP_5W_{30}\}$-**1** overlaps with the P-O vibration of the polyoxotungstate.[72] The P-O vibration of $\{Co_4(PW_9)_2\}$ occurs at 1030 cm^{-1} and is present in the spectrum of the nanoparticles.[84] The characteristic polyoxotungstate W-O vibrations arise at 1013 and 904 cm^{-1} in CMC-$\{NaP_5W_{30}\}$-**1**, and at 939 and 878 cm^{-1} in CMC-$\{Co_4(PW_9)_2\}$-**1**, respectively.[84,85] The minimal change in the position of the POM peaks in the nanoparticles compared to the pristine POM indicates no chemical changes to the POMs, suggesting that they are only physically entrapped. Likewise, the Raman spectra of the nanoparticles (Figures **S13**-**S15**) display the characteristic peaks of the POM nanoparticles, indicating their encapsulation. However, CMC signals are not observed.

For cryo-TEM analyses, CMC-$\{Co_4(PW_9)_2\}$-**1** nanoparticles were prepared with a concentration of 250 µM POM, centrifugal filtered, and washed with Milli-Q water. The

nanoparticles were then cryogenically frozen and subjected to TEM analysis (Figure **2**). The nanoparticles exhibit a spherical geometry with a diameter of ca. 200 nm, which agrees well with the DLS-determined average hydrodynamic radius of the particles of 156 nm (Table **S21**). The darker patches in the nanoparticle are likely to arise from the presence of the tungsten-rich polyoxometalates, but further evidence is required. The material around the nanoparticles is assumed to be collections of free CMC left over from the nanoparticle preparation, which were not separated by centrifugal filtration due to the large molecular weight of the polymer.

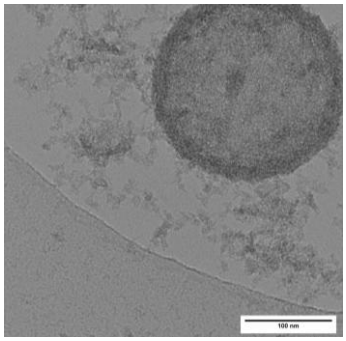

Figure 2. Cryo-TEM image of CMC-{$Co_4(PW_9)_2$}-**1** with a diameter of approximately 200 nm.

In addition, the stability of all CMC-{POM} nanoparticles was monitored through their change in size, as recorded by DLS (Table **S19**). In parallel, the absorbance of CMC-{$Co_4(PW_9)_2$}-**1** was measured with UV-vis spectroscopy (Figure **S30**).

ANTICANCER ACTIVITY

The influence of relevant POMs and nanocomposites on the viability of malignant and healthy cells was tested in vitro using a PrestoBlue assay. As PrestoBlue is non-toxic, the fluorescence measurement could be repeated if the control cells were not 100% confluent. In this work, we conducted two measurements, immediately after the end of the treatment and after an additional 24 h, and in one case also 48 and 72 h with fresh medium. This extended measurement allows for observations of both acute and protracted effects of the different compounds. These techniques were employed first to screen a series of POMs and then to probe the influence of CMC on POM cytotoxicity, either as a component of a mechanical mixture or as an encapsulant.

The activities of common tungstate species, Na_2WO_4, $H_3PW_{12}O_{40}$ {PW_{12}}, and $Na_9[PW_9O_{34}]${PW_9} were first tested on PC-3 cells (Figure **3**). Note that {PW_{12}} is not stable in the cell culture medium and several species are present according to ^{31}P-NMR spectroscopy monitoring (Figure **S31**).[26,28,86] The concentrations tested were normalized with respect to their tungsten contents to permit a better comparison of composition-activity trends. The tungsten concentrations of the three species ranged from 21,000 to 131 µM. The initial PrestoBlue reading showed that Na_2WO_4 was less cytotoxic than the POM species, exhibiting a statistically significant difference from the POMs for all concentrations except 2,625 µM tungsten (Figure **3** and Table **S4**). {PW_{12}} exhibited the greatest cytotoxicity of the three species, but this is only statistically significant at 5,250 µM and below (Figure **3** and Table **S4**).

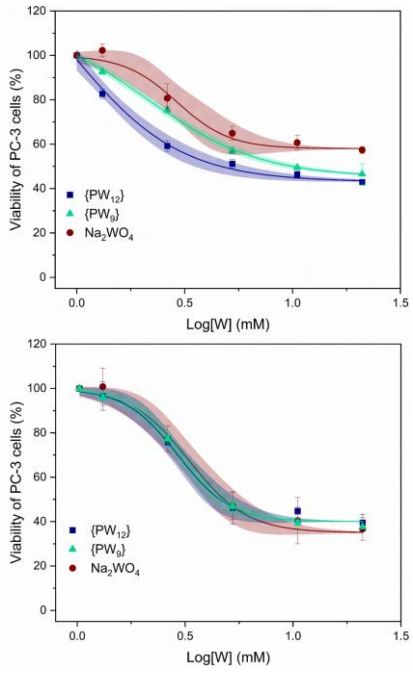

Figure 3. Dose-response curves for PC-3 cells treated with {PW_{12}} (blue), {PW_9} (green), and Na_2WO_4 (dark red) for 24 h (upper) and after an additional 24 h of incubation with fresh medium (lower).

After the allotted 24 h in fresh medium, only weak additional effects were observed, indicating that the majority of the effect arises during the initial POM incubation step. Nonetheless, partial recovery for cells treated with low concentrations of {PW_{12}} and a decrease in viability for cells treated with higher concentrations of Na_2WO_4 were observed. These minor changes lead to an overlap of the dose-response curves of all three tungstate species, indicating no statistically significant difference in the effects induced by each species (Figure **3** and Table **S5**). In summary, the three tungstate species exerted relatively weak biological effects that mostly occur immediately after treatment and exhibited very similar toxicities in the prolonged study; this may suggest that the species are unstable in the cells and either rearrange into the same structure motif or break down into smaller tungstate species, such as $(WO_4)^{2-}$.

Following these observations, we investigated two larger structures, {NaP_5W_{30}} and {$Co_4(PW_9)_2$}. The POMs were tested on the normal MRC-5 cell line with concentrations from 2,500 to 5 µM (Figure **4**) to obtain a baseline cytotoxicity for healthy cells. {NaP_5W_{30}} is starkly more cytotoxic towards the MRC-5 cells than {$Co_4(PW_9)_2$} (Figure **4** and Table **S6**). The calculated IC_{50} of {$Co_4(PW_9)_2$} is nearly 50 times higher than for {NaP_5W_{30}} (1). Fu *et al.* also observed that {NaP_5W_{30}} inhibited HT29 cells in a similar concentration range (Table **S2**)[37] and Geisberger *et al.* observed cytotoxicity of {$Co_4(PW_9)_2$} towards HeLa cells in a similar concentration range as applied in this study (Table **S2**).[40] Given our observation and comparisons to relevant literature,[37,40] we can infer that more tungsten atoms in a given POM increases the cytotoxicity. The cytotoxicity of the tungstate also is not outweighed by the four divalent cobalt centers, even though reference cobalt salts were found to be cytotoxic (Figure **S35**).

$\{Co_4(PW_9)_2\}$ is, nevertheless, found to be more cytotoxic than the $\{PW_9\}$ polyanion, which agrees with the work of Tan *et al.* which found that introducing three cobalt atoms in $Na_9[\{Na(H_2O)_2\}_3\{Co(H_2O)\}_3(\alpha\text{-B-}SbW_9O_{33})_2] \cdot 28H_2O$ increased the cytotoxicity compared to the precursor $Na_9[SbW_9O_{33}] \cdot 19.5H_2O$ (Table **S2**).[55]

We propose the application of CMC nanoparticles to improve the effectiveness of the POM as an anticancer agent. To this end, the encapsulation method described by Croce *et al.* was first applied for $\{NaP_5W_{30}\}$ and $\{Co_4(PW_9)_2\}$,[71] and the nanoparticle cytotoxicity was compared to that of the pristine POMs and a mixture of CMC and POM in solution. $CaCl_2$ and CMC nanoparticles without POM were found to be only partially cytotoxic (Figure **S33** and **S34**).

Figure **5** shows the dose-response curves for PC-3 cells treated with $\{NaP_5W_{30}\}$, CMC-$\{NaP_5W_{30}\}$-**1**, and a mixed solution of both CMC-**1** and $\{NaP_5W_{30}\}$ (CMC/$\{NaP_5W_{30}\}$). The mixed solution of CMC-**1** and POM was tested to determine whether the encapsulation provides further advantages beyond the mechanical combination. The POM concentration ranged from 500 to 2 µM while the CMC-**1** concentration in the nanoparticles and the mixture was 3.3 mg/mL. Combining $\{NaP_5W_{30}\}$ with CMC-**1** increases the cytotoxicity towards the PC-3 cells for concentrations of 15 µM or below (Figure **5**). Shah *et al.* similarly observed a slight increase in cytotoxicity of $(NH_4)_{14}[NaP_5W_{30}O_{110}]$ towards HeLa cells when encapsulated in chitosan for 10, 1, and 0.1 µM POM (Table **S2**).[38]

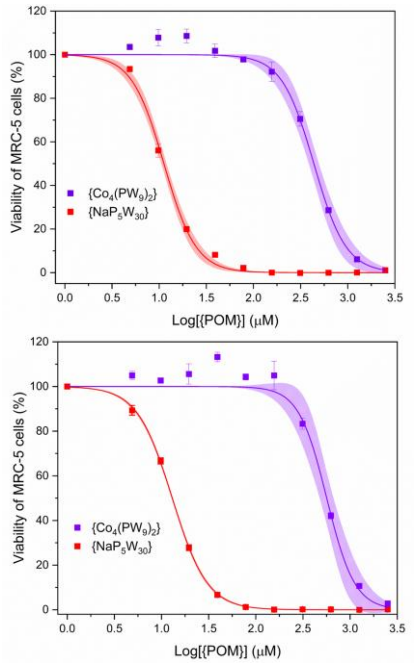

Figure 4. Dose-response curves for MRC-5 cells treated with $\{NaP_5W_{30}\}$ (red) and $\{Co_4(PW_9)_2\}$ (purple) for 24 h (upper) and after an additional 24 h of incubation with fresh medium (lower).

Further, in this test, all species at each concentration resulted in statistically significant differences except for when 31 µM was applied (Table **S8**). After 24 h, all values were statistically significant (Table **S9**). Additionally, the IC_{50} of the nanoparticles is almost three times lower than that of the pristine POM, while the IC_{50} of the mixture is predicted to be even lower but is out of the range of the experimental conditions (Table **S21**). Given that the Preyssler-type POM is persistently cytotoxic, even at low concentrations, and that the cytotoxicity is enhanced by encapsulation, obtaining a selective anticancer agent seemed unlikely and its investigation was not further pursued.

The method reported by Croce *et al.*[71] was further studied for the encapsulation of $\{Co_4(PW_9)_2\}$. CMC-$\{Co_4(PW_9)_2\}$-**1** nanoparticles were prepared and tested from 2500 to 52 µM POM on both HeLa and MRC-5 cells. The effect was compared to the pristine $\{Co_4(PW_9)_2\}$ and a mixture of CMC-**1** and $\{Co_4(PW_9)_2\}$ (CMC/$\{Co_4(PW_9)_2\}$) (Figure **6**). All the treatments resulted in a dose-dependent reduction in the viability for both cell lines after 24 h of treatment. The nanoparticle treatment was found to be slightly more cytotoxic for the HeLa cells than the pristine POM and the mixture; this effect was statistically significant at 188 µM for the POM and below 1056 µM for the mixture (excluding the outliers marked in red in Figure **6**) (Table **S10**).

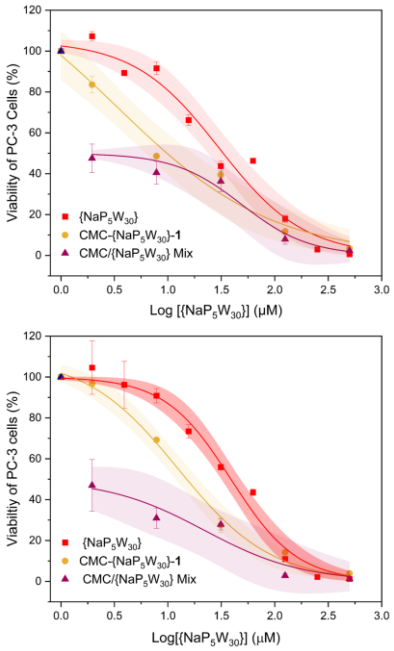

Figure 5. Dose-response curves for PC-3 cells treated with $\{NaP_5W_{30}\}$ (red), CMC-$\{NaP_5W_{30}\}$-**1** (gold), and CMC/$\{NaP_5W_{30}\}$ solution (burgundy) for 24 h (upper) and after an additional 24 h incubation with fresh medium (lower).

The second reading of the HeLa cells showed further reduction in viability when treated with the mixture or the nanoparticles (Figure **6**). Moreover, in the second reading, the effect of the mixture and the nanoparticles were significantly different below 1056 µM (Table **S11**). In the initial reading of the MRC-5 cells, the most cytotoxic reagent varied with concentration (Figure **6** and Table **S12**). After another 24 h, the effect of the mixture differentiated from that of the POM and the nanoparticles, exhibiting a statistically significant difference for all concentrations other than 687 and 52 µM (Table **S13**). The mixture showed greater cytotoxicity than the pristine POM and the nanoparticles with low to mid-range

concentrations, and showed a reduced effect compared to the POM and nanoparticles with higher concentrations. The nanoparticles, however, displayed the largest difference in the IC_{50} values for the HeLa and MRC-5 cell lines (Table **S22**).

Next, the encapsulation method employed by Geisberger *et al.*[40] was compared to our first method taken from Croce *et al*. The two encapsulation methods (CMC-{$Co_4(PW_9)_2$}-**1** and CMC-{$Co_4(PW_9)_2$}-**2**), as well as the mixture of CMC-**1** and {$Co_4(PW_9)_2$} (Figure **7**), were tested against PC-3 cells. It was observed immediately after treatment that the mixed solution was, with statistical significance (Table **S14**), more cytotoxic for the PC-3 cells than either nanoparticle system (**1** or **2**). After another 24 h, the remaining effects of the CMC-{$Co_4(PW_9)_2$}-**1** were the strongest while cells treated with lower concentrations of the mixed solution or CMC-{$Co_4(PW_9)_2$}-**2** were able to recover (Figure **7** and Table **S15**). This indicates that the conditions of combining CMC and POM are relevant for their cytotoxic effects.

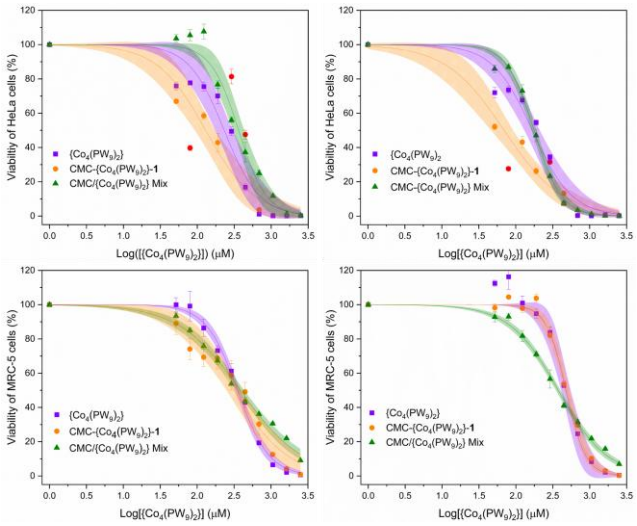

Figure 6. Upper: Dose-response curves of HeLa cells treated with {$Co_4(PW_9)_2$} (purple), CMC-{$Co_4(PW_9)_2$}-**1** (orange), and CMC/{$Co_4(PW_9)_2$} (green) for 24 h (left) and after an additional 24 h with fresh medium (right). The points in red are excluded from the fitting due to their irregularity. Lower: Dose-response curves of MRC-5 cells treated with the same species for 24 h (left) and after an additional 24 h with fresh medium (right).

Given the delayed effect on PC-3 cells induced by CMC-{$Co_4(PW_9)_2$}-**1**, we wanted to see how this changed with longer study times. For this reason, we repeated the treatment of PC-3 cells with CMC-{$Co_4(PW_9)_2$}-**1** as well as the pristine POM and checked the viability immediately after treatment, and 24, 48, and 72 h after treatment. We conducted the same experiment on MRC-5 cells, side by side to check for selectivity. The results are given in Figure **8**. PC-3 cells treated with CMC-{$Co_4(PW_9)_2$}-**1** showed statistically significant declines in the viability between the treatment and 24 h later but then rose again by 72 h after treatment, except in the case of the highest concentration tested (582 μM POM) (Figure **8**, Table **S16**). In comparison, PC-3 cells treated with {$Co_4(PW_9)_2$} experienced a declining trend in viability over the 72 h, resulting in statistically significant differences between the first and final readings for all concentrations from immediately after treatment to 72 h after treatment. On average, the opposite was true for MRC-5 cells. MRC-5 cells treated with nanoparticles and pristine POM experienced a significant recovery by 72 h after treatment. This is especially relevant for the highest concentration of nanoparticles (582 μM), for which MRC-5 cells could strongly recover by 72 h whereas the PC-3 cells at this same concentration reduced in viability with statistical significance from 71% after treatment to 20% after 72 h. Moreover, the extent of the recovery of the MRC-5 cells by 72 h is greater than that of the PC-3 cells at all other concentrations, despite the initially lower viability of the MRC-5 cells for all concentrations. Therefore, although PC-3 cells were found to slightly recover from the nanoparticle treatment after 48 h, MRC-5 cells could also meaningfully recover by the end of the assay. This both hints at the selectivity of our treatment and the necessity of longer assay times.

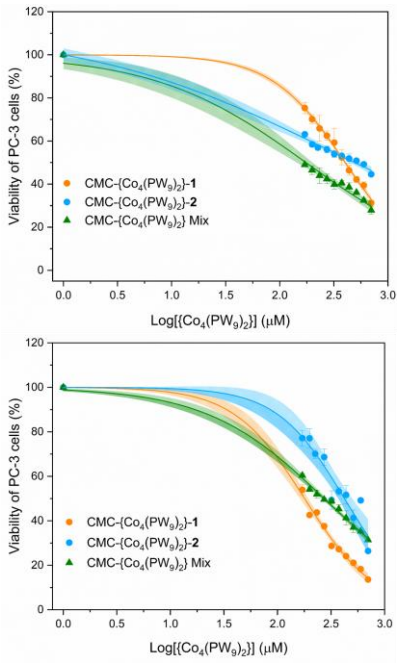

Figure 7. Dose-response curve of PC-3 cells treated with CMC-{$Co_4(PW_9)_2$}-**1** (orange), CMC-{$Co_4(PW_9)_2$}-**2** (blue), and with CMC/{$Co_4(PW_9)_2$} solution (green) for 24 h (upper) and after an additional 24 h with fresh medium (lower).

Figure **9** shows the results of HeLa and MRC-5 cells treated with the two nanoparticle systems (1 and 2, 700 to 50 μM POM). The motivation of this test was not only to investigate whether the nanoparticle type influences cytotoxicity but also whether the nanoparticles can also be selective towards HeLa cells. Both nanoparticle systems were observed to exhibit a dose-dependent cytotoxicity towards HeLa and MRC-5 cells (Figure **9** and Table S**17**). Specifically, the assay immediately after treatment showed that lower doses of CMC-{$Co_4(PW9)_2$}-**1** were non-toxic toward HeLa cells, while CMC-{$Co_4(PW_9)_2$}-**2** decreased the cell viability by more than 50% for all concentrations. The difference in the nanoparticles' effect was less pronounced for the MRC-5 cells but can still be observed. The viability of MRC-5 cells declined more steeply for cells treated with CMC-{$Co_4(PW_9)_2$}-**2** than CMC-{$Co_4(PW_9)_2$}-**1**. The influence of the nanosystem is also evident from the IC_{50} values, for which lower values are calculated for CMC-

{$Co_4(PW_9)_2$}-**2** than CMC-{$Co_4(PW_9)_2$}-**1** for both cell lines (Table **S21**). Interestingly, after an extra 24 h, the HeLa cell viability declined to nearly 0% for all concentrations while MRC-5 cells remained viable, indicating selectivity towards HeLa cells (Figure **9** and Table S**18**). This delayed effect on cancer cells was also observed for the PC-3 cells treated with CMC-{$Co_4(PW_9)_2$}-**1** (Figure **7**). Together, these observations of selectivity for cancer cells strongly support the use of extended viability studies, as some cell lines may take longer to fully react to the cytotoxicity of the nanoparticles.

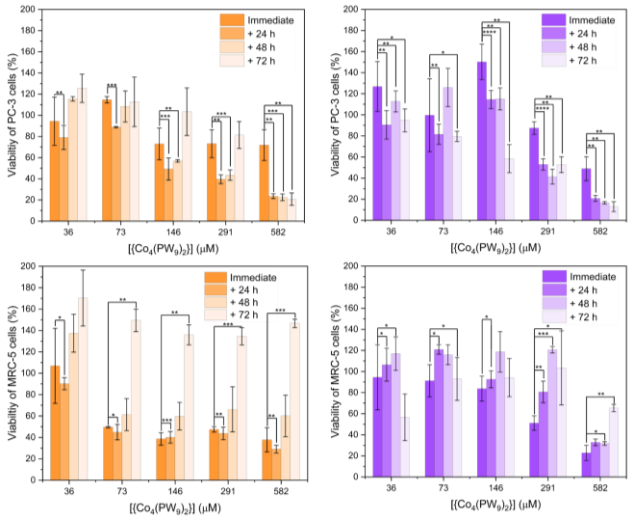

Figure 8. Extended viability assays (immediately, 24, 48, and 72 h after treatment) of PC-3 cells (upper) and MRC-5 cells (lower) treated with CMC-{$Co_4(PW_9)_2$}-**1** (left, orange) and {$Co_4(PW_9)_2$} (right, purple) for 24 h.

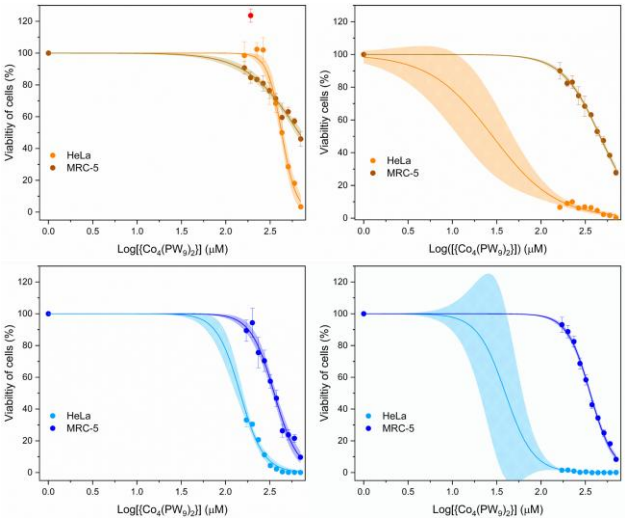

Figure 9. Upper: Dose-response curves of HeLa (orange) and MRC-5 cells (brown) treated with CMC-{$Co_4(PW_9)_2$}-**1** for 24 h (left) and after an additional 24 h with fresh medium (right). The point in red is excluded from the fitting due to irregularity. Lower: Dose-response curves of HeLa (light blue) and MRC-5 cells (dark blue) treated with CMC-{$Co_4(PW_9)_2$}-**2** for 24 h (left) and after an additional 24 h with fresh medium (right).

CONCLUSION

A series of bioactive and reference (polyoxo)tungstates, Na_2WO_4, $[PW_{12}O_{40}]^{3-}$, and $[PW_9O_{34}]^{9-}$, $[NaP_5W_{30}O_{110}]^{14-}$, and $[Co_4(H_2O)_2(PW_9O_{34})_2]^{10-}$, were prepared or used as purchased, characterized by FT-IR and Raman spectroscopy, PXRD, and ^{31}P-NMR, and first monitored for their stability and speciation. Three main research questions were in the focus, in short (a) exploration of cytotoxicity trends with respect to POM nuclearity and incorporated heteroatoms, (b) the influence of CMC encapsulation strategies on their cytotoxicity, and (c) cell viability after a rest period following treatment with POMs/nanoparticles. Among the investigated polyoxotungstates, $[NaP_5W_{30}O_{110}]^{14-}$ with the largest number of tungsten centers per molecule exhibited the highest cytotoxicity towards PC-3 at low molar concentrations. $[Co_4(H_2O)_2(PW_9O_{34})_2]^{10-}$ induced cytotoxicity with concentrations in a medium range, achieving IC_{50} values for MRC-5 cells of 437 ± 23 µM compared to 11 ± 0.3 µM for $[NaP_5W_{30}O_{110}]^{14-}$ determined in the same test. This and the other reference tests, answer our first research question, suggesting that POM size influences the cytotoxicity. More tungsten atoms lead to increased cytotoxicity even in comparison to the sandwich POM-containing inorganic cobalt(II) which is well known to be toxic.[87,88]

To address the second question concerning the effect of CMC on the POM cytotoxicity, we prepared and thoroughly characterized stable, spherical CMC-{$NaP_5W_{30}O_{110}$}-**1**, CMC-{$Co_4(PW_9O_{34})_2$}-**1** and CMC-{$Co_4(PW_9O_{34})_2$}-**2** nanoparticles, the latter two via different preparative pathways. The nanoparticles were then evaluated for their efficacy as anticancer agents and their activities were compared to the respective free POMs $[NaP_5W_{30}O_{110}]^{14-}$ and $[Co_4(H_2O)_2(PW_9O_{34})_2]^{10-}$ and to a mechanical mixture of free POM and CMC. Importantly, to address our third research question, whether a follow-up viability assay can provide additional vital information, the viability of the treated cells was investigated 24 h after treatment.

CMC typically increases the cytotoxicity of the POM towards the cancerous cell lines for $[NaP_5W_{30}O_{110}]^{14-}$ and $[Co_4(H_2O)_2(PW_9O_{34})_2]^{10-}$, regardless of whether it is applied as a component in a mixture or as an encapsulating macromolecule using either nanoparticle preparation method. To specifically address the role of the mode of encapsulation, CMC-{$Co_4(PW_9O_{34})_2$}-**1** and -**2** were compared on each cell line, leading mainly to statistically significant differences in their cytotoxicity. Also notable is that CMC-{$Co_4(PW_9O_{34})_2$}-**1** and -**2** are highly cytotoxic against HeLa cells compared to the normal MRC-5 cell line, especially in the second reading after 24 h. In comparison, PC-3 cells treated with CMC--{$Co_4(PW_9O_{34})_2$}-**2** partially recovered, whereas the viability of PC-3 cells treated with CMC-{$Co_4(PW_9O_{34})_2$}-**1** worsened. These results perfectly answer our final research question: follow-up viability assays can give a more comprehensive picture of the treatment effects, unveiling evidence of selectivity and cell recovery.

Our results therefore have a significant impact on future cytotoxicity studies on POM. Follow-up research must now be systematically conducted along these lines, including long-term viability studies with a wider array of POMs, nanocomposites, and cell lines to extend these conclusions to a larger scale and

to explore the structure-activity relations of POMs for their use as selective anticancer agents.

ACKNOWLEDGEMENT

This work was supported by the University of Zürich and the Swiss National Science Foundation (Grant No. 200021_200989). We thank Dr. Piotr Szwedziak and the staff of the Center for Microscopy and Image Analysis at the University of Zurich for assistance with cryo-TEM measurements. We are grateful to Theresa Lehmann (Institute of Anatomy, University of Zurich) for her assistance and advice regarding the cell assays.

AUTHOR INFORMATION

Corresponding Author

greta.patzke@chem.uzh.ch
caroline.maake@anatomy.uzh.ch

Author Contributions

The manuscript was written through contributions of all authors. All authors have given approval to the final version of the manuscript. ‡These authors contributed equally.

REFERENCES

(1) Wild, C. P.; Weiderpass, E.; Stewart, B. W. *World Cancer Report*:*Cancer research for cancer prevention*.

(2) Hanahan, D.; Weinberg, R. A. Hallmarks of cancer: the next generation. *Cell* **2011**, *144* (5), 646–674. DOI: 10.1016/j.cell.2011.02.013.

(3) Alderden, R. A.; Hall, M. D.; Hambley, T. W. The Discovery and Development of Cisplatin. *J. Chem. Educ.* **2006**, *83* (5), 728. DOI: 10.1021/ed083p728.

(4) Rosenberg, B. Charles F. Kettring prize. Fundamental studies with cisplatin. *Cancer* **1985**, *55* (10), 2303–2316. DOI: 10.1002/1097-0142(19850515)55:10<2303:AID-CNCR2820551002>3.0.CO;2-L.

(5) Gandin, V.; Hoeschele, J. D.; Margiotta, N. Special Issue "Cisplatin in Cancer Therapy: Molecular Mechanisms of Action 3.0". *Int. J. Mol. Sci.* **2023**, *24* (9). DOI: 10.3390/ijms24097917.

(6) Lippert, B., Ed. *Cisplatin: Chemistry and biochemistry of a leading anticancer drug*; Helvetica Chimica Acta, 2006.

(7) Zamble, D. B.; Lippard, S. J. Cisplatin and DNA repair in cancer chemotherapy. *Trends Biochem. Sci.* **1995**, *20* (10), 435–439. DOI: 10.1016/S0968-0004(00)89095-7.

(8) Gumerova, N. I.; Rompel, A. Synthesis, structures and applications of electron-rich polyoxometalates. *Nat. Rev. Chem.* **2018**, *2* (0112). DOI: 10.1038/s41570-018-0112.

(9) Pope, M. T.; Müller, A. Polyoxometalate Chemistry: An Old Field with New Dimensions in Several Disciplines. *Angew. Chem. Int. Ed. Engl.* **1991**, *30* (1), 34–48. DOI: 10.1002/anie.199100341.

(10) Song, Y.-F.; Tsunashima, R. Recent advances on polyoxometalate-based molecular and composite materials. *Chem. Soc. Rev.* **2012**, *41* (22), 7384–7402. DOI: 10.1039/c2cs35143a.

(11) Bijelic, A.; Aureliano, M.; Rompel, A. The antibacterial activity of polyoxometalates: structures, antibiotic effects and future perspectives. *Chem. Commun.* **2018**, *54* (10), 1153–1169. DOI: 10.1039/C7CC07549A.

(12) Bijelic, A.; Aureliano, M.; Rompel, A. Polyoxometalates as Potential Next-Generation Metallodrugs in the Combat Against Cancer. *Angew. Chem. Int. Ed.* **2019**, *58* (10), 2980–2999. DOI: 10.1002/anie.201803868.

(13) Rhule, J. T.; Hill, C. L.; Judd, D. A. Polyoxometalates in Medicine. *Chem. Rev.* **1998**, *98* (1), 327–358. DOI: 10.1021/cr960396q.

(14) Čolović, M. B.; Lacković, M.; Lalatović, J.; Mougharbel, A. S.; Kortz, U.; Krstić, D. Z. Polyoxometalates in Biomedicine: Update and Overview. *Curr. Med. Chem.* **2020**, *27* (3), 362–379. DOI: 10.2174/0929867326666190827153532.

(15) Stojanović, M.; Čolović, M. B.; Lalatović, J.; Milosavljević, A.; Savić, N. D.; Declerck, K.; Radosavljević, B.; Ćetković, M.; Kravić-Stevović, T.; Parac-Vogt, T. N.; Krstić, D. Monolacunary Wells-Dawson Polyoxometalate as a Novel Contrast Agent for Computed Tomography: A Comprehensive Study on In Vivo Toxicity and Biodistribution. *Int. J. Mol. Sci.* **2024**, *25* (5), 2569. DOI: 10.3390/ijms25052569.

(16) Lentink, S.; Salazar Marcano, D. E.; Moussawi, M. A.; Parac-Vogt, T. N. Exploiting Interactions between Polyoxometalates and Proteins for Applications in (Bio)chemistry and Medicine. *Angew. Chem. Int. Ed.* **2023**, *62* (31), e202303817. DOI: 10.1002/ange.202303817.

(17) Yamase, T.; Fujita, H.; Fukushima, K. Medical chemistry of polyoxometalates. Part 1. Potent antitumor activity of polyoxomolybdates on animal transplantable tumors and human cancer xenograft. *Inorg. Chim. Acta* **1988**, *151* (1), 15–18. DOI: 10.1016/S0020-1693(00)83477-5.

(18) Ogata, A.; Yanagie, H.; Ishikawa, E.; Morishita, Y.; Mitsui, S.; Yamashita, A.; Hasumi, K.; Takamoto, S.; Yamase, T.; Eriguchi, M. Antitumour effect of polyoxomolybdates: induction of apoptotic cell death and autophagy in in vitro and in vivo models. *Br. J. Cancer* **2008**, *98* (2), 399–409. DOI: 10.1038/sj.bjc.6604133.

(19) Yamase, T.; Tomita, K. Medical chemistry of polyoxometalates Part 3. Electrochemical study of a 1:1 polyoxomolybdate-flavin mononucleotide complex in aqueous solutions. *Inorg. Chim. Acta* **1990**, *169* (2), 147–150. DOI: 10.1016/S0020-1693(00)80509-5.

(20) Pope, M. T., Müller, A., Ed. *Polyoxometalates: From Platonic Solids to Anti-Retroviral Activity*; Topics in Molecular Organization and Engineering, Vol. 10; Springer, Dodrecht, 1994. DOI: 10.1007/978-94-011-0920-8_25.

(21) Fujita, H.; Fujita, T.; Sakurai, T.; Yamase, T.; Seto, Y. Antitumor activity of new antitumor substance, polyoxomolybdate, against several human cancers in athymic nude mice. *Tohoku J. Exp. Med.* **1992**, *168* (2), 421–426. DOI: 10.1620/tjem.168.421.

(22) Fujita, H.; Fujita, T.; Sakurai, T.; Seto, Y. A New Type of Antitumor Substances; Polyoxomolybdates. *Chemotherapy* **1992**, *40* (2), 173–178. DOI: 10.11250/chemotherapy1953.40.173.

(23) Mitsui, S.; Ogata, A.; Yanagie, H.; Kasano, H.; Hisa, T.; Yamase, T.; Eriguchi, M. Antitumor activity of polyoxomolybdate, $[NH_3Pr^i]_6[Mo_7O_{24}] \cdot 3H_2O$, against, human gastric cancer model. *Biomed. Pharmacother.* **2006**, *60* (7), 353–358. DOI: 10.1016/j.biopha.2006.02.009.

(24) Ogata, A.; Mitsui, S.; Yanagie, H.; Kasano, H.; Hisa, T.; Yamase, T.; Eriguchi, M. A novel anti-tumor agent, polyoxomolybdate induces apoptotic cell death in AsPC-1 human pancreatic cancer cells. *Biomed. Pharmacother.* **2005**, *59* (5), 240–244. DOI: 10.1016/j.biopha.2004.11.008.

(25) Liu, Y.; Tian, S.; Liu, S.; Wang, E. In vitro inhibitory effect of polyoxometalates on human tumor cells. *Transit. Met. Chem.* **2005**, *30* (1), 113–117. DOI: 10.1007/s11243-004-3825-1.

(26) Gumerova, N. I.; Rompel, A. Speciation atlas of polyoxometalates in aqueous solutions. *Sci. Adv.* **2023**, *9* (25), eadi0814. DOI: 10.1126/sciadv.adi0814.

(27) Long, D.-L.; Streb, C.; Song, Y.-F.; Mitchell, S.; Cronin, L. Unravelling the complexities of polyoxometalates in solution using mass spectrometry: protonation versus heteroatom inclusion. *J. Am. Chem. Soc.* **2008**, *130* (6), 1830–1832. DOI: 10.1021/ja075940z.

(28) Gumerova, N. I.; Rompel, A. Polyoxometalates in solution: speciation under spotlight. *Chem. Soc. Rev.* **2020**, *49* (21), 7568–7601. DOI: 10.1039/D0CS00392A.

(29) Lampl, R.; Breibeck, J.; Gumerova, N. I.; Galanski, M. S.; Rompel, A. Wells-Dawson phosphotungstates as mushroom tyrosinase inhibitors: a speciation study. *Sci. Rep.* **2021**, *11* (1), 19354. DOI: 10.1038/s41598-021-96491-5.

(30) Zou, Y.-L.; Li, H.-Y.; Zhou, W.; Cui, X.-G.; Zou, G.-H.; Shen, G.-Z. Introduction of the antibacterial drugs norfloxacin and

Ciprofloxacin into a polyoxometalate structure: Synthesis, characterization, and antibacterial activity. *J. Mol. Struct.* **2020**, *1205*, 127584. DOI: 10.1016/j.molstruc.2019.127584.
(31) Sachdeva, S.; Maret, W. Comparative outcomes of exposing human liver and kidney cell lines to tungstate and molybdate. *Toxicol. Mech. Methods* **2021**, *31* (9), 690–698. DOI: 10.1080/15376516.2021.1956031.
(32) Khader, A.; Sherman, L. S.; Rameshwar, P.; Arinzeh, T. L. Sodium Tungstate for Promoting Mesenchymal Stem Cell Chondrogenesis. *Stem Cells Dev.* **2016**, *25* (24), 1909–1918. DOI: 10.1089/scd.2016.0158.
(33) Sha, J.-Q.; Liang, L.-Y.; Li, X.; Zhang, Y.; Yan, H.; Chen, G. Ligation of the quinolone antibacterial agent pipemidic acid to Keggin polyoxotungstates. *Polyhedron* **2011**, *30* (10), 1657–1662. DOI: 10.1016/j.poly.2011.03.044.
(34) Zhou, Z.; Zhang, D.; Yang, L.; Ma, P.; Si, Y.; Kortz, U.; Niu, J.; Wang, J. Nona-copper(II)-containing 18-tungsto-8-arsenate(III) exhibits antitumor activity. *Chem. Commun.* **2013**, *49* (45), 5189–5191. DOI: 10.1039/C3CC41628C.
(35) Wu, Q.; Ju, H.; Tao, J.; Chen, Z.; Li, J.; Wang, F.; Cai, Q.; Sun, L.; Pan, X. New Member of Organic Ligand Functionalized TMSP: Synthesis, Characterized and Properties of $Na_{15}[(Mn^{II}(COOH))_3(AsW_9O_{33})_2]\cdot 15H_2O$. *J. Clust. Sci.* **2015**, *26* (5), 1811–1820. DOI: 10.1007/s10876-015-0880-z.
(36) Tan, R.; Wang, C.; Cui, S.; Wang, H.; Han, J.; Xie, R. Synthesis, Crystal Structure and Antitumor Activities of a New Cobalt-containing Tungstoantimonate $Na_9[\{Na(H_2O)_2\}\{Co(H_2O)\}_3(\alpha\text{-B-}SbW_9O_{33})_2]\cdot 28H_2O$. *J. Macromol. Sci., Part A* **2014**, *51* (1), 33–36. DOI: 10.1080/10601325.2014.850621.
(37) Fu, L.; Gao, H.; Yan, M.; Li, S.; Li, X.; Dai, Z.; Liu, S. Polyoxometalate-Based Organic-Inorganic Hybrids as Antitumor Drugs. *Small* **2015**, *11* (24), 2938–2945. DOI: 10.1002/smll.201500232.
(38) Shah, H. S.; Al-Oweini, R.; Haider, A.; Kortz, U.; Iqbal, J. Cytotoxicity and enzyme inhibition studies of polyoxometalates and their chitosan nanoassemblies. *Toxicol. Rep.* **2014**, *1*, 341–352. DOI: 10.1016/j.toxrep.2014.06.001.
(39) Razavi, S. F.; Bamoharram, F. F.; Hashemi, T.; Shahrokhabadi, K.; Davoodnia, A. Nanolipid-loaded Preyssler polyoxometalate: Synthesis, characterization and invitro inhibitory effects on HepG2 tumor cells. *Toxicol. In Vitro* **2020**, *68*, 104917. DOI: 10.1016/j.tiv.2020.104917.
(40) Geisberger, G.; Paulus, S.; Carraro, M.; Bonchio, M.; Patzke, G. R. Synthesis, characterisation and cytotoxicity of polyoxometalate/carboxymethyl chitosan nanocomposites. *Chem. Eur.* **2011**, *17* (16), 4619–4625. DOI: 10.1002/chem.201002815.
(41) León, I. E.; Porro, V.; Astrada, S.; Egusquiza, M. G.; Cabello, C. I.; Bollati-Fogolin, M.; Etcheverry, S. B. Polyoxometalates as antitumor agents: Bioactivity of a new polyoxometalate with copper on a human osteosarcoma model. *Chem. Biol. Interact.* **2014**, *222*, 87–96. DOI: 10.1016/j.cbi.2014.10.012.
(42) Haider, A.; Zarschler, K.; Joshi, S. A.; Smith, R. M.; Lin, Z.; Mougharbel, A. S.; Herzog, U.; Müller, C. E.; Stephan, H.; Kortz, U. Preyssler-Pope-Jeannin Polyanions $[NaP_5W_{30}O_{110}]^{14-}$ and $[AgP_5W_{30}O_{110}]^{14-}$: Microwave-Assisted Synthesis, Structure, and Biological Activity. *Z. Anorg. Allg. Chem.* **2018**, *644* (14), 752–758. DOI: 10.1002/zaac.201800113.
(43) Faleiro, L.; Marques, A.; Martins, J.; Jordão, L.; Nogueira, I.; Gumerova, N. I.; Rompel, A.; Aureliano, M. The Preyssler-Type Polyoxotungstate Exhibits Anti-Quorum Sensing, Antibiofilm, and Antiviral Activities. *Biology* **2022**, *11* (7), 994. DOI: 10.3390/biology11070994.
(44) Shah, H. S.; Joshi, S. A.; Haider, A.; Kortz, U.; ur-Rehman, N.; Iqbal, J. Synthesis of chitosan-coated polyoxometalate nanoparticles against cancer and its metastasis. *RSC Adv.* **2015**, *5* (113), 93234–93242. DOI: 10.1039/C5RA18489D.
(45) Yin, Q.; Tan, J. M.; Besson, C.; Geletii, Y. V.; Musaev, D. G.; Kuznetsov, A. E.; Luo, Z.; Hardcastle, K. I.; Hill, C. L. A fast soluble carbon-free molecular water oxidation catalyst based on abundant metals. *Science* **2010**, *328* (5976), 342–345. DOI: 10.1126/science.1185372.
(46) Zhu, G.; Lv, H.; Vickers, J. W.; Geletii, Y. V.; Luo, Z.; Song, J.; Huang. Structural and mechanistic studies of tunable, stable, fast multi-cobalt water oxidation catalysts. In *Solar Hydrogen and Nanotechnology VI*; Tachibana, Y., Ed.; SPIE, 2011, Vol. 8109; 8109A. DOI: 10.1117/12.894024.
(47) Munteanu, C. R.; Suntharalingam, K. Advances in cobalt complexes as anticancer agents. *Dalton Trans.* **2015**, *44* (31), 13796–13808. DOI: 10.1039/c5dt02101d.
(48) Dolbecq, A.; Dumas, E.; Mayer, C. R.; Mialane, P. Hybrid organic-inorganic polyoxometalate compounds: from structural diversity to applications. *Chem. Rev.* **2010**, *110* (10), 6009–6048. DOI: 10.1021/cr1000578.
(49) Anyushin, A. V.; Kondinski, A.; Parac-Vogt, T. N. Hybrid polyoxometalates as post-functionalization platforms: from fundamentals to emerging applications. *Chem. Soc. Rev.* **2020**, *49* (2), 382–432. DOI: 10.1039/C8CS00854J.
(50) Boulmier, A.; Feng, X.; Oms, O.; Mialane, P.; Rivière, E.; Shin, C. J.; Yao, J.; Kubo, T.; Furuta, T.; Oldfield, E.; Dolbecq, A. Anticancer Activity of Polyoxometalate-Bisphosphonate Complexes: Synthesis, Characterization, In Vitro and In Vivo Results. *Inorg. Chem.* **2017**, *56* (13), 7558–7565. DOI: 10.1021/acs.inorgchem.7b01114.
(51) Saad, A.; Zhu, W.; Rousseau, G.; Mialane, P.; Marrot, J.; Haouas, M.; Taulelle, F.; Dessapt, R.; Serier-Brault, H.; Rivière, E.; Kubo, T.; Oldfield, E.; Dolbecq, A. Polyoxomolybdate Bisphosphonate Heterometallic Complexes: Synthesis, Structure, and Activity on a Breast Cancer Cell Line. *Chemistry* **2015**, *21* (29), 10537–10547. DOI: 10.1002/chem.201406565.
(52) Geisberger, G.; Paulus, S.; Gyenge, E. B.; Maake, C.; Patzke, G. R. Targeted delivery of polyoxometalate nanocomposites. *Small* **2011**, *7* (19), 2808–2814. DOI: 10.1002/smll.201101264.
(53) Zhang, J.; Huang, Y.; Li, G.; Wei, Y. Recent advances in alkoxylation chemistry of polyoxometalates: From synthetic strategies, structural overviews to functional applications. *Coord. Chem. Rev.* **2019**, *378*, 395–414. DOI: 10.1016/j.ccr.2017.10.025.
(54) Yan, Y.; Zhang, J.; Ren, L.; Tang, C. Metal-containing and related polymers for biomedical applications. *Chem. Soc. Rev.* **2016**, *45* (19), 5232–5263. DOI: 10.1039/c6cs00026f.
(55) Wang, X.; Liu, J.; Li, J.; Yang, Y.; Liu, J.; Li, B.; Pope, M. T. Synthesis and antitumor activity of cyclopentadienyltitanium substituted polyoxotungstate $CoW_{11}O_{39}(CpTi)^{7-}$ ($Cp=eta_5\text{-}C_5H_5$). *J. Inorg. Biochem.* **2003**, *94* (3), 279–284. DOI: 10.1016/S0162-0134(02)00631-1.
(56) Dong, Z.; Tan, R.; Cao, J.; Yang, Y.; Kong, C.; Du, J.; Zhu, S.; Zhang, Y.; Lu, J.; Huang, B.; Liu, S. Discovery of polyoxometalate-based HDAC inhibitors with profound anticancer activity in vitro and in vivo. *Eur. J. Med. Chem.* **2011**, *46* (6), 2477–2484. DOI: 10.1016/j.ejmech.2011.03.036.
(57) Guo, R.; Cheng, Y.; Ding, D.; Li, X.; Zhang, L.; Jiang, X.; Liu, B. Synthesis and antitumoral activity of gelatin/polyoxometalate hybrid nanoparticles. *Macromol. Biosci.* **2011**, *11* (6), 839–847. DOI: 10.1002/mabi.201000434.
(58) Dianat, S.; Bordbar, A. K.; Tangestaninejad, S.; Yadollahi, B.; Zarkesh-Esfahani, S. H.; Habibi, P. *In vitro* antitumor activity of parent and nano-encapsulated mono cobalt-substituted Keggin polyoxotungstate and its ctDNA binding properties. *Chem. Biol. Interact.* **2014**, *215*, 25–32. DOI: 10.1016/j.cbi.2014.02.011.
(59) Dianat, S.; Bordbar, A.-K.; Tangestaninejad, S.; Yadollahi, B.; Amiri, R.; Zarkesh-Esfahani, S.-H.; Habibi, P. In vitro antitumor activity of free and nano-encapsulated $Na_5[PMo_{10}V_2O_{40}]\cdot nH_2O$ and its binding properties with ctDNA by using combined spectroscopic methods. *J. Inorg. Biochem.* **2015**, *152*, 74–81. DOI: 10.1016/j.jinorgbio.2015.08.015.
(60) Dianat, S.; Bordbar, A. K.; Tangestaninejad, S.; Zarkesh-Esfahani, S. H.; Habibi, P.; Abbasi Kajani, A. ctDNA interaction of Co-containing Keggin polyoxomolybdate and in vitro antitumor

activity of free and its nano-encapsulated derivatives. *J. Iran. Chem. Soc.* **2016**, *13* (10), 1895–1904. DOI: 10.1007/s13738-016-0906-y.
(61) Mishra, M. K., Ed. *Handbook of encapsulation and controlled release*; CRC Press, 2016.
(62) Wang, X.; Liu, J.; Pope, M. T. New polyoxometalate/starch nanomaterial: synthesis, characterization and antitumoral activity. *Dalton Trans.* **2003** (5), 957–960. DOI: 10.1039/b300920n.
(63) Zhai, F.; Li, D.; Zhang, C.; Wang, X.; Li, R. Synthesis and characterization of polyoxometalates loaded starch nanocomplex and its antitumoral activity. *Eur. J. Med. Chem.* **2008**, *43* (9), 1911–1917. DOI: 10.1016/j.ejmech.2007.11.032.
(64) Kickelbick, G. Concepts for the incorporation of inorganic building blocks into organic polymers on a nanoscale. *Prog. Polym. Sci.* **2003**, *28* (1), 83–114. DOI: 10.1016/S0079-6700(02)00019-9.
(65) Kruse, J.-H.; Langer, M.; Romanenko, I.; Trentin, I.; Hernández-Castillo, D.; González, L.; Schacher, F. H.; Streb, C. Polyoxometalate-Soft Matter Composite Materials: Design Strategies, Applications, and Future Directions. *Adv. Funct. Mater.* **2022**, *32* (51). DOI: 10.1002/adfm.202208428.
(66) Ali, A.; Ahmed, S. A review on chitosan and its nanocomposites in drug delivery. *Int. J. Biol. Macromol.* **2018**, *109*, 273–286. DOI: 10.1016/j.ijbiomac.2017.12.078.
(67) Ravi Kumar, M. N. A review of chitin and chitosan applications. *React. Funct. Polym.* **2000**, *46* (1), 1–27. DOI: 10.1016/S1381-5148(00)00038-9.
(68) Saikia, C.; Gogoi, P.; Maji, T. K. Chitosan: A Promising Biopolymer in Drug Delivery Applications. *J. Mol. Genet. Med.* **2015**, *s4*. DOI: 10.4172/1747-0862.S4-006.
(69) Zhang, E.; Xing, R.; Liu, S.; Qin, Y.; Li, K.; Li, P. Advances in chitosan-based nanoparticles for oncotherapy. *Carbohydr. Polym.* **2019**, *222*, 115004. DOI: 10.1016/j.carbpol.2019.115004.
(70) Shariatinia, Z. Carboxymethyl chitosan: Properties and biomedical applications. *Int. J. Biol. Macromol.* **2018**, *120, Part B*, 1406–1419. DOI: 10.1016/j.ijbiomac.2018.09.131.
(71) Croce, M.; Conti, S.; Maake, C.; Patzke, G. R. Nanocomposites of Polyoxometalates and Chitosan-Based Polymers as Tuneable Anticancer Agents. *Eur. J. Inorg. Chem.* **2019**, *2019* (3-4), 348–356. DOI: 10.1002/ejic.201800268.
(72) Creaser, I.; Heckel, M. C.; Neitz, R. J.; Pope, M. T. Rigid nonlabile polyoxometalate cryptates $[ZP_5W_{30}O_{110}]^{(15-n)-}$ that exhibit unprecedented selectivity for certain lanthanide and other multivalent cations. *Inorg. Chem.* **1993**, *32* (9), 1573–1578. DOI: 10.1021/ic00061a010.
(73) Evans, H. T.; Tourné, G. F.; Tourné, C. M.; Weakley, T. J. R. X-Ray Crystallographic and Tungsten-183 Nuclear Magnetic Resonance Structural Studies of the $[M_4(H_2O)_2(XW_9O_{34})_2]^{10-}$ Heteropolyanions (M = Co^{ii} or Zn, X = P or As). *J. Chem. Soc., Dalton Trans.* **1986** (12), 2699–2705. DOI: 10.1039/DT9860002699.
(74) Finke, R. G.; Droege, M. W.; Domaille, P. J. Trivacant Heteropolytungstate Derivatives. 3. Rational Syntheses, Characterization, Two-Dimensional ^{183}W NMR, and Properties of $P_2W_{18}M_4(H_2O)_2O_{68}^{10-}$ and $P_4W_{30}M_4(H_2O)_2O_{112}^{16-}$ (M = Co, Cu, Zn). *Inorg. Chem.* **1987**, *26* (23), 3886–3896. DOI: 10.1021/ic00270a014.
(75) Chen, X.-G.; Park, H.-J. Chemical characteristics of O-carboxymethyl chitosans related to the preparation conditions. *Carbohydr. Polym.* **2003**, *53* (4), 355–359. DOI: 10.1016/S0144-8617(03)00051-1.
(76) Shi, X.; Du, Y.; Yang, J.; Zhang, B.; Sun, L. Effect of degree of substitution and molecular weight of carboxymethyl chitosan nanoparticles on doxorubicin delivery. *J. Appl. Polym. Sci.* **2006**, *100* (6), 4689–4696. DOI: 10.1002/app.23040.
(77) Muzzarelli, R. A.; Ilari, P.; Petrarulo, M. Solubility and structure of N-carboxymethylchitosan. *Int. J. Biol. Macromol.* **1994**, *16* (4), 177–180. DOI: 10.1016/0141-8130(94)90048-5.
(78) Abreu, F. R. de; Campana-Filho, S. P. Preparation and characterization of carboxymethylchitosan. *Polímeros* **2005**, *15* (2), 79–83. DOI: 10.1590/S0104-14282005000200004.
(79) Hill, C. L.; Weeks, M. S.; Schinazi, R. F. Anti-HIV-1 Activity, Toxicity, and Stability Studies of Representative Structural Families of Polyoxometalates. *J. Med. Chem.* **1990**, *33* (10), 2767–2772. DOI: 10.1021/jm00172a014.
(80) Grama, L.; Boda, F.; Gaz Florea, A. S.; Curticăpean, A.; Muntean, D.-L. The UV and IR Comparative Spectrophotometric Study of Some Saturated and Lacunary Polyoxometalates. *Acta Med. Marisiensis* **2014**, *60* (3), 84–88. DOI: 10.2478/amma-2014-0017.
(81) Farag, R. K.; Mohamed, R. R. Synthesis and characterization of carboxymethyl chitosan nanogels for swelling studies and antimicrobial activity. *Molecules* **2012**, *18* (1), 190–203. DOI: 10.3390/molecules18010190.
(82) Britto, D. de; Campana-Filho, S. P. A kinetic study on the thermal degradation of N,N,N-trimethylchitosan. *Polym. Degrad. Stab.* **2004**, *84* (2), 353–361. DOI: 10.1016/j.polymdegradstab.2004.02.005.
(83) Anitha, A.; Divya Rani, V. V.; Krishna, R.; Sreeja, V.; Selvamurugan, N.; Nair, S. V.; Tamura, H.; Jayakumar, R. Synthesis, characterization, cytotoxicity and antibacterial studies of chitosan, O-carboxymethyl and N,O-carboxymethyl chitosan nanoparticles. *Carbohydr. Polym.* **2009**, *78* (4), 672–677. DOI: 10.1016/j.carbpol.2009.05.028.
(84) Limani, N.; Marques, I. S.; Jarrais, B.; Fernandes, A. J. S.; Freire, C.; Fernandes, D. M. Cobalt Phosphotungstate-Based Composites as Bifunctional Electrocatalysts for Oxygen Reactions. *Catalysts* **2022**, *12* (4), 357. DOI: 10.3390/catal12040357.
(85) Trakarnpruk, W.; Wannatem, A.; Kongpeth, J. Sandwich-type Cobalt Tungstophosphate: Synthesis, Characterization and Catalytic Activity. *JMMM* **2015**, *25* (1). DOI: 10.14456/jmmm.2015.1.
(86) Maksimovskaya, R. I.; Maksimov, G. M. ^{31}P NMR studies of hydrolytic conversions of 12-tungstophosphoric heteropolyacid. *Coord. Chem. Rev.* **2019**, *385*, 81–89.
(87) Simonsen, L. O.; Harbak, H.; Bennekou, P. Cobalt metabolism and toxicology--a brief update. *Sci. Total Environ.* **2012**, *432*, 210–215. DOI: 10.1016/j.scitotenv.2012.06.009.
(88) Paustenbach, D. J.; Tvermoes, B. E.; Unice, K. M.; Finley, B. L.; Kerger, B. D. A review of the health hazards posed by cobalt. *Crit. Rev. Toxicol.* **2013**, *43* (4), 316–362. DOI: 10.3109/10408444.2013.779633.